Synthetic lipid membrane channels formed by designed DNA nanostructures

Martin Langecker[1,†], **Vera Arnaut**[1,†], **Thomas G. Martin**[2,†], **Jonathan List**[1], **Stephan Renner**[1], **Michael Mayer**[3], **Hendrik Dietz**[2,*], and **Friedrich C. Simmel**[1,*]

[1]Lehrstuhl für Bioelektronik, Physics Department and ZNN/WSI, Technische Universität München, Am Coulombwall 4a, 85748 Garching, Germany

[2]Center for Integrated Protein Science at the Walter Schottky Institute, Technische Universität München, James-Franck-Straße 1, 85748 Garching, Germany

[3]Department of Biomedical Engineering, University of Michigan, Ann Arbor, Michigan 48109, USA

Abstract

We created nanometer-scale transmembrane channels in lipid bilayers using self-assembled DNA-based nanostructures. Scaffolded DNA origami was used to create a stem that penetrates and spans a lipid membrane, and a barrel-shaped cap that adheres to the membrane in part via 26 cholesterol moieties. In single-channel electrophysiological measurements, we find similarities to the response of natural ion channels, such as conductances on the order of 1 nS and channel gating. More pronounced gating was seen for mutations in which a single DNA strand of the stem protruded into the channel. In single-molecule translocation experiments, we highlight one of many potential applications of the synthetic channels, namely as single DNA molecule sensing devices.

A large class of proteins and peptides form channels through lipid bilayer membranes (1) to facilitate the transport of water, ions, or other entities through the otherwise impermeable membranes. Here, we report on a synthetic membrane channel that is constructed entirely from DNA and anchored to a lipid membrane with cholesterol side chains. The shape of our synthetic channel is inspired by the natural channel protein α-hemolysin (2), but it differs from it in its physical properties such as charge, hydrophobicity, and size. We constructed the channel using molecular self-assembly with scaffolded DNA origami (3–9) (Fig. 1A). The channel consists of two modules: a stem that penetrates and spans a lipid membrane, and a barrel-shaped cap that adheres to the (cis)-side of the membrane. Adhesion to the lipid bilayer is mediated by 26 cholesterol moieties that are attached to the cis-facing surface of the barrel (Fig. 1A). The stem protrudes centrally from the barrel and consists of six double-helical DNA domains that form a hollow tube. The interior of this tube acts as a transmembrane channel with a diameter of ≈ 2 nm and a length of ≈ 42 nm and runs through both stem and barrel (Fig. 1 B and C).

---

*Correspondence to: dietz@tum.de, simmel@tum.de.
†These authors contributed equally to this work.

Transmission electron microscopy (TEM) images taken from purified structures (Fig. 1D) confirmed that the intended shape is realized (SOM text S1, Figs. S1–S2) (10). Experiments with unilamellar lipid vesicles show that the synthetic DNA channels bind to lipid bilayer membranes (Fig. 1E,F,G and SOM text S2, Figs. S4–S8) in the desired orientation in which the cholesterol-modified face of the barrel forms tight contact with the membrane and the stem appears to protrude into the lipid bilayer (Fig. 1F, Fig. S9).

These observations suggested that the synthetic DNA channels could form membrane pores as designed. As the energetic cost for insertion of the charged DNA structure into the hydrophobic core of the lipid membrane would be prohibitively high, membrane penetration is thought to involve reorganization of the lipid bilayer around the charged stem structure, with the hydrophilic lipid headgroups oriented towards the DNA structure (cf. discussion in SOM text S3).

In order to demonstrate the electrical conductivity of the resulting membrane pores, we performed single-channel electrophysiological experiments (11) using an integrated chip-based setup (Fig. S14) (12). We added synthetic DNA channels at low concentrations (≈ 200 pM) to the cis side of the setup and applied voltage pulses to facilitate incorporation into the membrane (13, 14) (fig. S11A). As with biological channels, successful membrane incorporation of individual synthetic DNA channels manifested itself in a stepwise increase in transmembrane current (Fig. 2A) along with an increase in electrical noise (fig. S11B). Depending on the preparation method, we also observed incorporation of multiple DNA channels into the same membrane (fig. S13). The synthetic DNA channels displayed an average Ohmic conductance of $G = 0.87 \pm 0.15$ nS (I = 174 pA at 200 mV) per channel in a solution containing 1 M KCl and 2 mM $MgCl_2$ (Fig. 2B,C). A simple geometrical model (1) predicts $G = 0.78$ nS for a channel with diameter 2 nm and length 42 nm (SOM text S4) which agrees favorably with what we observe.

Many natural ion channels display current gating caused by switching between distinct channel conformations with different conductances (1). The synthetic DNA channels also displayed gating behavior (Fig. 2D, trace i–iii), which may be caused by thermal fluctuations of the structure. We hypothesized that stochastic unzipping and rezipping of short double-helical DNA domains in the channel may also contribute to the observed current gating. To test this idea we designed three channel 'mutants' that differed from the 'wild type' channel only by a single-stranded heptanucleotide protruding from the central transmembrane tube (Fig. 1B, SOM text S6). The mutant channels showed more pronounced gating than wildtype channels (Fig. 2D, trace iv-vi), and they also significantly differed in their gating time statistics (Fig. 2E, fig. S16). Every investigated mutant channel displayed gating, while some of the wildtype channels did not show gating at all (Fig. 2D, trace i). The transmembrane current hence depended on fine structural details of the synthetic DNA channel.

In the past, nanoscale membrane pores have shown great potential for the use as single molecule biosensors (15–22), whose operation principle is based on the transient blockage of ionic current by analyte molecules. The type of sensing task that can be accomplished with such 'nanopores' depends on their size and their chemical structure. Nanopore sensors based on naturally occurring membrane pores provide excellent electrical properties, but altering the geometry of biological pores and introducing chemical functions through genetic engineering or chemical conjugation is challenging. By contrast, the geometry of synthetic DNA objects (23, 24) and their chemical properties (24) can be tailored for custom nanopore sensing applications. Here, we used our synthetic DNA lipid membrane channel for single-molecule studies of DNA hairpin unzipping and guanine quadruplex (25) unfolding. Single-stranded DNA is expected to fit through the 2 nm wide central pore of the DNA channel,

while larger DNA secondary structures such as hairpins or quadruplexes are not (26, 27). In order to translocate through the DNA channel, the structures need to unzip or unfold as in similar experiments with α-hemolysin, thus providing a characteristic time delay in the current blockades that reveals the kinetics of structural transitions (26–28).

For one set of experiments, we used a DNA hairpin with a 9 base pair long stem flanked by 50 thymidines on the $3'$ end and 6 thymidines on the $5'$ end (Fig. 3A). The hairpin molecules were initially added to the cis side of a lipid membrane containing a single synthetic DNA channel that displayed a stable current baseline without gating. Application of a positive voltage bias leads to capture, unzipping, and translocation of the hairpin structures resulting in transient current blockades (Fig. 3A,B). Reversal of the bias after approximately ≈ 30 minutes again led to transient current blockades, this time caused by molecules that had accumulated in the trans compartment by previous translocation through the DNA channel. The blockade amplitudes for both translocation directions were $\Delta I_{cis\text{-}trans}$ = 11.9 ± 2.7 pA and $\Delta I_{trans\text{-}cis}$ = 20.3 ± 4.2 pA. The blockade dwell times were distributed exponentially with a characteristic lifetime of $\tau_{cis\text{-}trans}$ = 1.5 ms and $\tau_{trans\text{-}cis}$ = 1 ms, respectively (Fig. 3C).

In another set of experiments, we added quadruplex-forming oligonucleotides with a 60 thymidine long single-stranded tail (Q-T60) to the cis side of a membrane containing a single synthetic DNA channel (Fig. 3D,E). Again, we observed transient current blockades, which correspond to the capture and threading of quadruplex DNA molecules into the channel, followed by unfolding and subsequent translocation through the pore. Removal of the analyte from the cis compartment restored a stable baseline current without blockades. Subsequent addition of quadruplex DNA with a longer $(dT)_{125}$ tail (Q-T125) led to larger current blockades. The average current blockades were $\Delta I_{Q\text{-}T60}$ = 5.6 ± 1.0 pA and $\Delta I_{Q\text{-}T125}$ = 15.3 ± 2.3 pA, respectively. The larger current blockade for Q-T125 as compared to Q-T60 translocations can be explained by the larger volume occupied in the channel by the longer T_{125} tail as compared to the T_{60} tail (SOM text S7). The blockade dwell times are distributed exponentially with characteristic lifetimes of $\tau_{Q\text{-}T60}$ = 9.7 ms and $tQ\tau_{Q\text{-}T125}$ = 8.1 ms. Thus, similar to biological pores our synthetic DNA channels can be used as sensing devices to discriminate analyte molecules by studying their translocation characteristics.

In addition to single molecule sensing, the synthetic DNA channels introduced here open up broad perspectives for applications as antimicrobial agents and interference with cellular homeostasis. More generally, we believe that fully synthetic lipid membrane channels are a crucial first step towards harnessing ion flux for driving sophisticated nanodevices that are inspired by the rich functional diversity of natural membrane machines such as ion pumps, rotary motors, and transport proteins.

Supplementary Material

Refer to Web version on PubMed Central for supplementary material.

Acknowledgments

MM, HD, FCS designed the research. ML, VA, SR performed electrophysiological experiments. TM prepared the synthetic DNA channels and performed TEM. JL, VA, TM performed experiments with lipid vesicles. HD, FCS wrote the paper. All authors discussed the results and commented on the manuscript.

References and Notes

1. Hille, B. Ion channels of excitable membranes. 3. Sinauer Associates; Sunderland: 2001.

2. Song L, et al. Structure of staphylococcal alpha-hemolysin, a heptameric transmembrane pore. Science. Dec 13.1996 274:1859. [PubMed: 8943190]

3. Rothemund PWK. Folding DNA to create nanoscale shapes and patterns. Nature. Mar 16.2006 440:297. [PubMed: 16541064]

4. Douglas SM, et al. Self-assembly of DNA into nanoscale three-dimensional shapes. Nature. May 21.2009 459:414. [PubMed: 19458720]

5. Andersen ES, et al. Self-assembly of a nanoscale DNA box with a controllable lid. Nature. Feb 19.2009 459:73. [PubMed: 19424153]

6. Dietz H, Douglas SM, Shih WM. Folding DNA into Twisted and Curved Nanoscale Shapes. Science. Aug.2009 325:725. [PubMed: 19661424]

7. Seeman NC. Nanomaterials Based on DNA. Annu Rev Biochem. Jun 7.2010 79:65. [PubMed: 20222824]

8. Han D, et al. DNA origami with complex curvatures in three-dimensional space. Science. Apr 15.2011 332:342. [PubMed: 21493857]

9. Castro CE, et al. A primer to scaffolded DNA origami. Nat Meth. 2011; 8:221.

10. Materials and methods are available as supporting material on Science Online.

11. Sakmann, B.; Neher, E. Single Channel Recording. Plenum; New York: 1995.

12. Baaken G, Sondermann M, Schlemmer C, Ruehe J, Behrends JC. Planar microelectrode-cavity array for high-resolution and parallel electrical recording of membrane ionic currents. Lab Chip. Jan 1.2008 8:938. [PubMed: 18497915]

13. Danelon C, Nestorovich EM, Winterhalter M, Ceccarelli M, Bezrukov SM. Interaction of Zwitterionic Penicillins with the OmpF Channel Facilitates Their Translocation. Biophys J. Jan 3.2006 90:1617. [PubMed: 16339889]

14. Renner S, Bessonov A, Simmel FC. Voltage-controlled insertion of single alpha-hemolysin and Mycobacterium smegmatis nanopores into lipid bilayer membranes. Appl Phys Lett. 2011; 1

15. Kasianowicz JJ, Brandin E, Branton D, Deamer DW. Characterization of individual polynucleotide molecules using a membrane channel. Proc Natl Acad Sci U S A. Nov 26.1996 93:13770. [PubMed: 8943010]

16. Bayley H, Cremer PS. Stochastic sensors inspired by biology. Nature. Sep 13.2001 413:226. [PubMed: 11557992]

17. Howorka S, Siwy Z. Nanopore analytics: sensing of single molecules. Chem Soc Rev. Jan 1.2009 38:2360. [PubMed: 19623355]

18. Dekker C. Solid-state nanopores. Nature Nanotechnology. Apr.2007 2:209.

19. Hall AR, et al. Hybrid pore formation by directed insertion of [alpha]-haemolysin into solid-state nanopores. Nat Nano. 2010; 5:874.

20. Branton D, et al. The potential and challenges of nanopore sequencing. Nat Biotech. Oct 1.2008 26:1146.

21. Majd S, et al. Applications of biological pores in nanomedicine, sensing, and nanoelectronics. Curr Opin Biotech. Jan 1.2010 21:439. [PubMed: 20561776]

22. Manrao EA, et al. Reading DNA at single-nucleotide resolution with a mutant MspA nanopore and phi29 DNA polymerase. Nat Biotech. Jan 4.2012 30:349.

23. Bell NAW, et al. DNA Origami Nanopores. Nano Lett. Jan 1.2012 12:512. [PubMed: 22196850]

24. Wei R, Martin TG, Rant U, Dietz H. DNA Origami Gatekeepers for Solid-State Nanopores. Angewandte Chemie International Edition. 2012:n/a.

25. Burge S, Parkinson GN, Hazel P, Todd AK, Neidle S. Quadruplex DNA: sequence, topology and structure. Nucleic Acids Res. 2006

26. Vercoutere W, et al. Rapid discrimination among individual DNA hairpin molecules at single-nucleotide resolution using an ion channel. Nat Biotech. 2001; 19:248.

27. Sauer-Budge AF, Nyamwanda JA, Lubensky DK, Branton D. Unzipping kinetics of double-stranded DNA in a nanopore. Phys Rev Lett. 2003; 90:238101. [PubMed: 12857290]

28. Mathe J, Visram H, Viasnoff V, Rabin Y, Meller A. Nanopore Unzipping of Individual DNA Hairpin Molecules. Biophys J. 2004; 87:3205. [PubMed: 15347593]
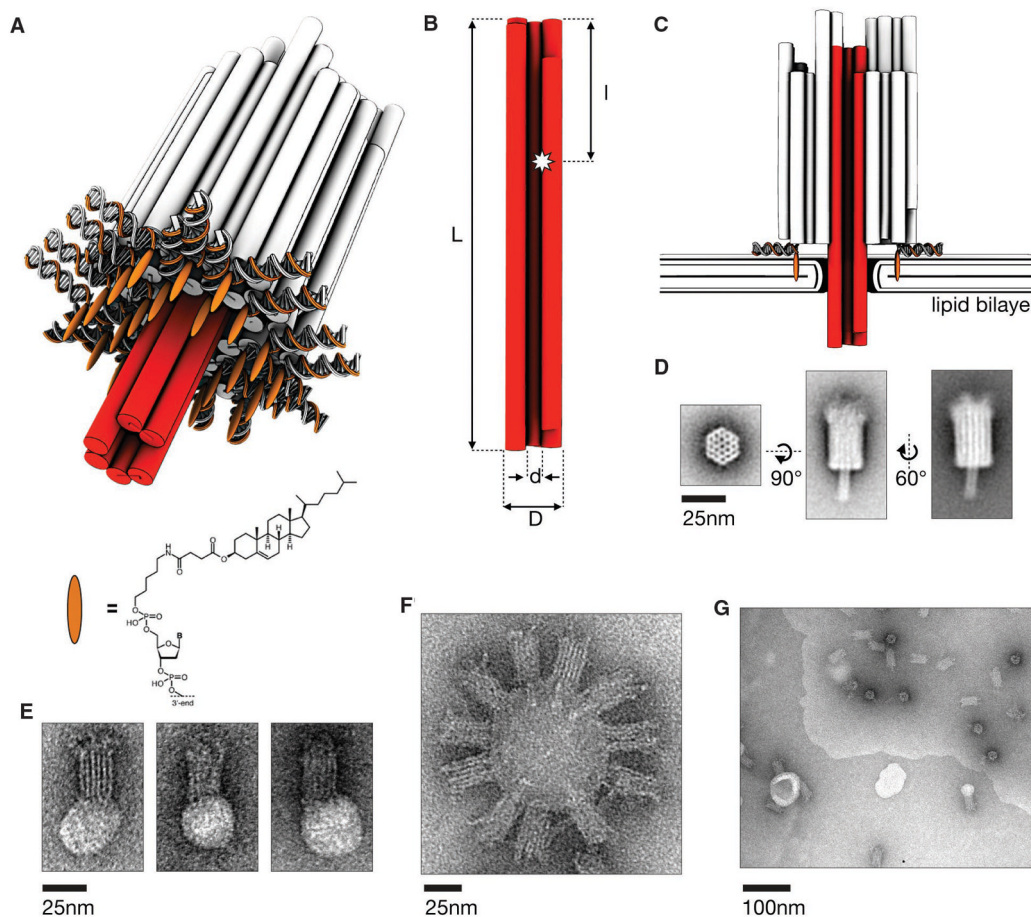
Fig. 1.
Synthetic DNA membrane channels. **(A)** Schematic illustration of the channel formed by 54 double-helical DNA domains packed on a honeycomb lattice. Cylinders indicate double-helical DNA domains. Red: transmembrane stem. Orange strands with orange ellipsoids indicate cholesterol-modified oligonucleotides that hybridize to single-stranded DNA adaptor strands. **(B)** Geometric specifications of the transmembrane channel. Length L = 47 nm, tube diameter D = 6 nm, inner diameter d = 2 nm. The length of the central channel fully surrounded by DNA helices is 42 nm. The star symbol indicates the position of a 7 base strand extension acting as a 'defect' in channel 'mutants' (l=15 nm for mutant M1 and l=14 nm for mutant M2, cf. SOM text S6, and caDNAno maps Figs. S22–24). **(C)** Cross-sectional view through the channel when incorporated in a lipid bilayer. **(D)** Averaged negative-stain TEM images obtained from purified DNA channel structures (class averages obtained from raw images displayed in Fig. S1,S2). **(E),(F)** Examples for TEM images of DNA channels adhering to small unilamellar vesicles (SUVs) made from POPC (1-palmitoyl-2-oleoyl-sn-glycero-3-phosphocholine) lipids. More images and a statistical analysis of vesicle size distribution and binding efficiency are found in SOM text S2 (Figs. S4–S9). **(G)** TEM image of DNA channels binding to an extended lipid bilayer in the upper right part of the image. DNA channels are found predominantly on lipid covered areas or sticking to SUVs (cf. SOM text S2).
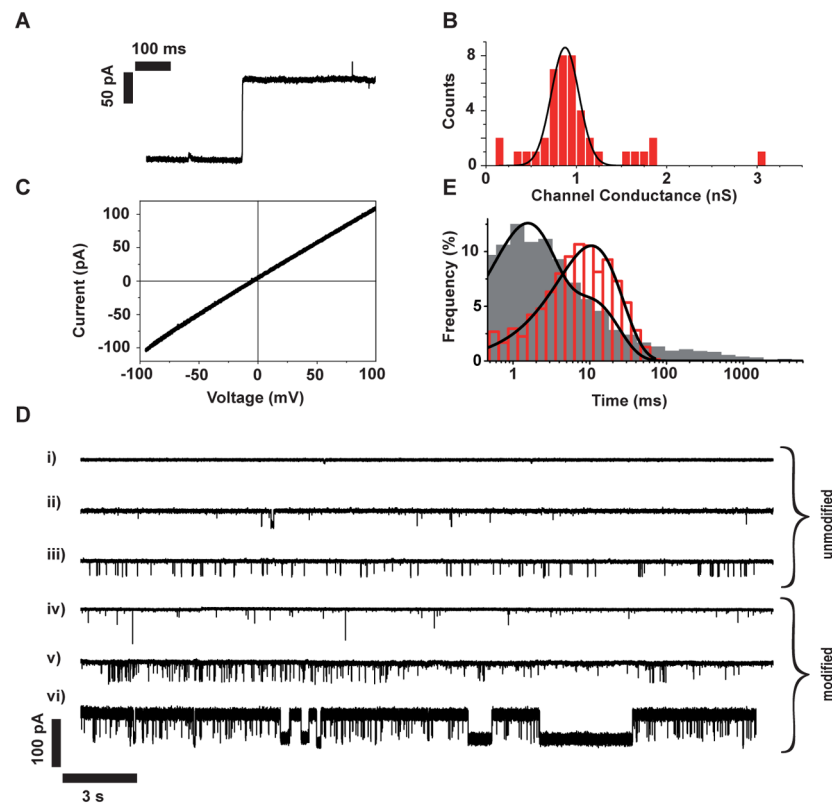
Fig. 2.
Electrical characterization performed on painted DPhPC (1,2-diphytanoyl-sn-glycero-3-phosphocholine) bilayers on a chip-based electrophysiology setup. **(A)** Stepwise increase in ionic current during an incorporation event at V=200 mV. **(B)** Histogram of channel conductances obtained from 43 incorporation events. The black line depicts a Gaussian fit. **(C)** Current – voltage dependence of the channel after incorporation. **(D)** Typical current traces obtained from 'wildtype' channels (i–iii), and 'mutants' with modification M2 (iv-vi, cf. SOM text S6). **(E)** Statistics of gating times for the wildtype (red) and the mutant (gray) channels. Continuous lines correspond to a mono-exponential fit for the wildtype channel ($\tau=10.5$ ms) and a double-exponential fit for the mutant ($\tau_1=1.3$ ms and $\tau_2=9.2$ ms).
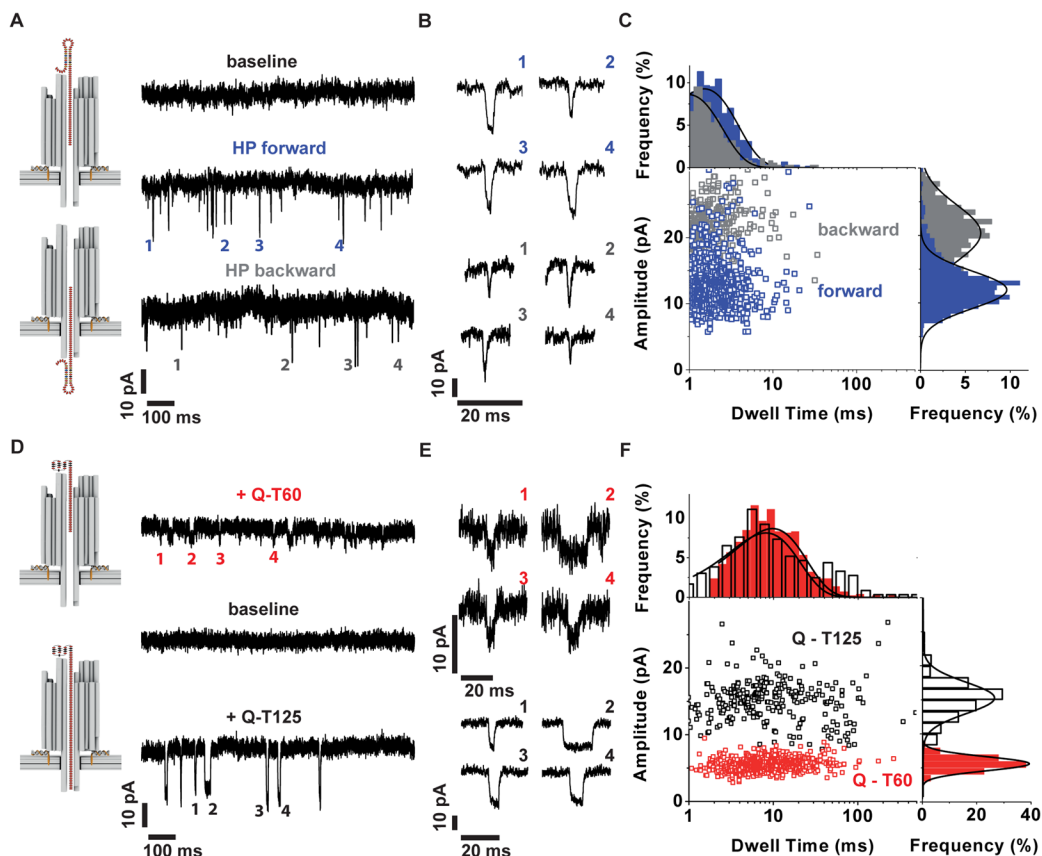
Fig. 3.

DNA Translocation studies. **(A)** Addition of DNA hairpins (T5-HP-T50) to a DNA channel at V=200 mV results in the appearance of current blockades, indicating unzipping and translocation of hairpin molecules from cis to trans. Hairpins accumulated on the trans side can also be transferred back from trans to cis by a reversal of the transmembrane voltage. **(B)** Representative blockade events for forward (top) and backward (bottom) translocation of DNA hairpins. **(C)** Scatter plot for the translocation of T5-HP-T50 DNA through a DNA channel from cis to trans (blue) and from trans to cis side (gray) at V=200 mV, and corresponding histograms. Each data point corresponds to a single translocation event. In total, 777 (forward) and 379 (backward) events were analyzed. **(D)** Top: Typical current trace at V=200 mV after addition of 10 μM of Q-T60 DNA. Middle: Current trace after rinsing with buffer solution. Bottom: Current trace after subsequent addition of 10 μM of Q-T125 DNA to the same channel. **(E)** Representative blockade events for Q-T60 (top) and Q-T125 DNA (bottom). **(F)** Scatter plot of the current blockade versus dwell time for the translocation of Q-T60 (red) and Q-T125 DNA (black) through the DNA channel. In total 631 (Q-T60) and 279 (Q-T125) events were analyzed. On the right and on the top corresponding histograms are shown. The lines correspond to single exponential (top) and Gaussian fits (right).